MARTIN MARIETTA ENERGY SYSTEMS LIBRARIES
3 4456 0361207 1

[redacted]

CENTRAL RESEARCH LIBRARY
DOCUMENT COLLECTION

AEC RESEARCH AND DEVELOPMENT REPORT

ORNL-2425
C-84 - Reactors-Special
Features of Aircraft Reactors

cy. 4A

ART REFLECTOR TEMPERATURE DISTRIBUTION

D. L. Platus
D. M. Miller
R. V. Meghreblian

DECLASSIFIED

CLASSIFICATION CHANGED TO:
BY AUTHORITY OF: E. J. Murphy 12-1-59
BY: M. Fallert 1-19-60

CENTRAL RESEARCH LIBRARY
DOCUMENT COLLECTION
LIBRARY LOAN COPY
DO NOT TRANSFER TO ANOTHER PERSON
If you wish someone else to see this document, send in name with document and the library will arrange a loan.

OAK RIDGE NATIONAL LABORATORY
OPERATED BY
UNION CARBIDE NUCLEAR COMPANY
Division of Union Carbide Corporation
UCC
POST OFFICE BOX X · OAK RIDGE, TENNESSEE

[redacted]

This [redacted] defined in the [redacted] disclosure of its contents in any manner to an unauthorized person is prohibited.

[redacted]

LEGAL NOTICE

This report was prepared as an account of Government sponsored work. Neither the United States, nor the Commission, nor any person acting on behalf of the Commission:

A. Makes any warranty or representation, express or implied, with respect to the accuracy, completeness, or usefulness of the information contained in this report, or that the use of any information, apparatus, method, or process disclosed in this report may not infringe privately owned rights; or

B. Assumes any liabilities with respect to the use of, or for damages resulting from the use of any information, apparatus, method, or process disclosed in this report.

As used in the above, "person acting on behalf of the Commission" includes any employee or contractor of the Commission to the extent that such employee or contractor prepares, handles or distributes, or provides access to, any information pursuant to his employment or contract with the Commission.

MARTIN MARIETTA ENERGY SYSTEMS LIBRARIES
3 4456 0361208 0

X-826

[redacted]

CENTRAL RESEARCH LIBRARY
DOCUMENT COLLECTION

OAK RIDGE NATIONAL LABORATORY
Operated by
UNION CARBIDE NUCLEAR COMPANY
Division of Union Carbide Corporation
UCC
Post Office Box X
Oak Ridge, Tennessee

C-84 Aircraft Reactors

ERRATA

to

ORNL- 2425

DATE: May 7, 1958

COPY NO.

"This document consists of 3 pages.
No. 5 of 280 copies, Series A"

SUBJECT: ART REFLECTOR TEMPERATURE DISTRIBUTION, by D. L. Platus, D. M. Miller, R. V. Meghreblian

TO: Distribution of ORNL-2425

FROM: J. R. Tallackson

DECLASSIFIED
CLASSIFICATION CHANGED TO:
BY AUTHORITY OF: E. J. Murphy 11-18-59
BY: Sm. Tallent 1-19-60

Revised pages 18 and 29 for ORNL-2425.

CENTRAL RESEARCH LIBRARY
DOCUMENT COLLECTION
LIBRARY LOAN COPY
DO NOT TRANSFER TO ANOTHER PERSON
If you wish someone else to see this document, send in name with document and the library will arrange a loan.

[redacted]

[redacted]

HEAT TRANSFER CALCULATIONS

1. Subdivision of Reflector Into Slab Elements. The following system of nomenclature will be used:

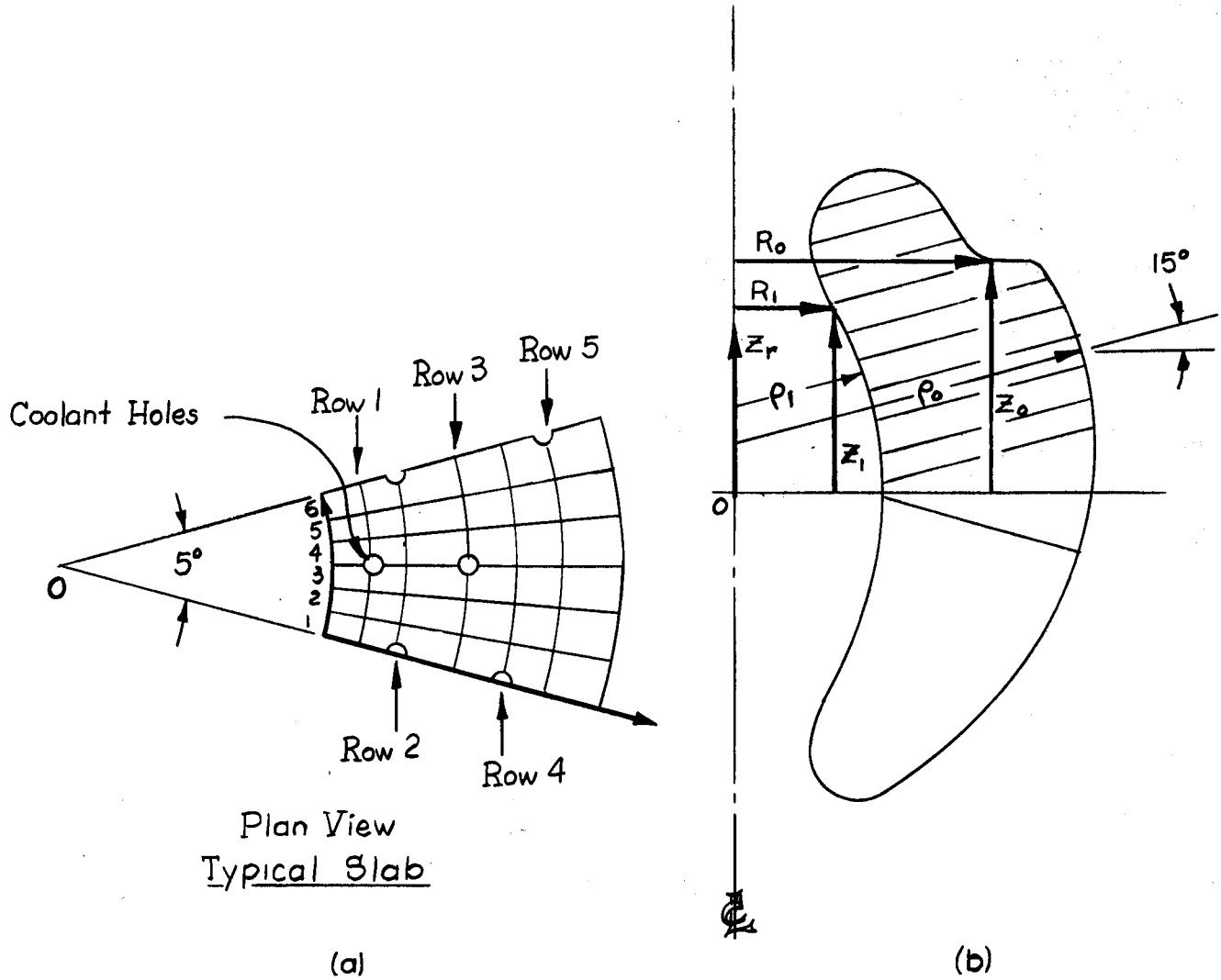

Fig. 8 Nomenclature of Slabs

All slabs except 1, 11, 22 are 1.75-in. thick. Slab 1 is 1-in. thick, slab 11 is a wedge with variable thickness, and slab 22 is 0.75-in. thick. The numbering of the slabs runs from the top of the Be reflector to the bottom. All slabs except 11 are inclined 15° to the equator. In this manner the slabs will be perpendicular to the cooling passages. The radial distance, ρ, is always measured from the reactor's vertical centerline. A 5° cut of the total reflector is always used in the solution of the problem. This 5° will be subdivided into six parts as shown by the j

MARTIN MARIETTA ENERGY SYSTEMS LIBRARIES
3 4456 0361208 0

Appendix I

Basic Slab Data

Slab	log ρ_i	ρ_i	log ρ_o	ρ_o	R_i-in	R_o-in	R_{avg}	Z_1-in	Z_o-in	Z_{avg}	Temp-°F inside annulus	Temp-°F outside annulus	ΔT
1	1.8720	6.50	2.3560	10.54	6.28	10.18	8.19	15.45	16.45	+15.95	1050	1050	0
2	1.9210	6.83	2.5470	12.76	6.60	12.32	9.46	14.05	15.60	+14.83	1058	1050	8
3	2.0000	7.39	2.6430	14.05	7.14	13.57	10.36	12.40	14.15	+13.28	1061	1080	19
4	2.0820	8.02	2.7190	15.16	7.75	14.64	11.20	10.75	12.60	+11.68	1067	1110	43
5	2.1630	8.70	2.7700	15.95	8.40	15.41	11.91	9.25	10.95	+10.10	1072	1140	68
6	2.2390	9.39	2.9860	19.81	9.07	19.13	14.10	7.65	10.10	+ 8.88	1077	1250	173
7	2.3100	10.07	3.0020	20.12	9.73	19.43	14.58	6.00	8.60	+ 7.30	1082	1246	164
8	2.3620	10.61	3.0190	20.46	10.25	19.76	15.01	4.30	7.00	+ 5.65	1090	1244	154
9	2.3400	10.38	3.0810	21.78	10.03	21.04	15.54	2.65	5.35	+ 4.00	1098	1241	143
10	2.4130	11.17	3.0990	22.17	10.79	21.41	16.10	0.90	3.70	+ 2.30	1105	1238	133
11[1]	2.3890	10.90	3.0860	21.88	10.90	21.88	16.39	0.00	0.00	000	1112	1235	123
12	2.4130	11.17	3.0990	22.17	10.79	21.41	16.10	- 0.90	- 3.70	- 2.30	1117	1231	114
13	2.3400	10.38	3.0810	21.78	10.03	21.04	15.54	- 2.65	- 5.35	- 4.00	1125	1227	102
14	2.3620	10.61	3.0190	20.46	10.25	19.76	15.01	- 4.30	- 7.00	- 5.65	1135	1223	88
15	2.3100	10.07	3.0020	20.12	9.73	19.43	14.58	- 6.00	- 8.60	- 7.30	1143	1219	76
16	2.2390	9.39	2.9860	19.81	9.07	19.13	14.10	- 7.65	-10.10	- 8.88	1151	1216	65
17	2.1630	8.70	2.9370	18.87	8.40	18.23	13.32	- 9.65	-10.95	-10.30	1158	1213	55
18	2.0820	8.02	2.875	17.73	7.75	17.13	12.44	-10.75	-12.60	-11.68	1166	1210	44
19	2.0000	7.39	2.8000	16.45	7.14	15.89	11.52	-12.40	-14.70	-13.55	1171	1207	36
20	1.9210	6.83	2.7900	16.28	6.60	15.72	11.16	-14.05	-16.10	-15.08	1177	1205	28
21	1.8560	6.40	2.5650	13.00	6.18	12.56	9.37	-15.95	-17.55	-16.75	1183	1205	22
22	1.8900	6.62	2.4620	11.72	6.39	11.32	8.86	-17.20	-18.40	-17.80	1185	1202	17
23	1.8410	6.30	2.3030	10.00	6.09	9.66	7.88	-18.35	-19.20	-18.78	1189	1199	10

Note: Values of R and ρ include portions of the coolant sodium in the inner and outer annuli and hence do not duplicate the exact dimensions of reflector.

1. All slabs except Slab 11 are inclined 15° to the equator; therefore, Slab 11 excepted, $R=\rho \cos 15°$. (See Figs 8 and 15, pp 18 and 24)

[redacted]

ORNL-2425 [redacted]

This document consists of 43 pages.
Copy 4 of 280 copies. Series A.

Contract No. W-7405-eng-26

REACTOR PROJECTS DIVISION

ART REFLECTOR TEMPERATURE DISTRIBUTION

D. L. Platus
D. M. Miller
R. V. Meghreblian

DATE ISSUED

FEB 19 1958

OAK RIDGE NATIONAL LABORATORY
Operated by
UNION CARBIDE NUCLEAR COMPANY
A Division of Union Carbide Corporation
Post Office Box X
Oak Ridge, Tennessee

[redacted]

[redacted]

[redacted]

3 4456 0361207 1

INTERNAL DISTRIBUTION

1. C. E. Center
2. Biology Library
3. Health Physics Library
4-5. Central Research Library
6. Reactor Experimental Engineering Library
7-11. Laboratory Records Department
12. Laboratory Records, ORNL R.C.
13. L. B. Emlet (K-25)
14. J. P. Murray (Y-12)
15. R. G. Affel
16. L. G. Alexander
17. C. J. Barton
18. M. Bender
19. D. S. Billington
20. F. F. Blankenship
21. E. P. Blizard
22. A. L. Boch
23. C. J. Borkowski
24. W. F. Boudreau
25. M. A. Bredig
26. E. J. Breeding
27. R. B. Briggs
28. W. E. Browning
29. F. R. Bruce
30. A. D. Callihan
31. D. W. Cardwell
32. R. A. Charpie
33. R. L. Clark
34. C. E. Clifford
35. J. H. Coobs
36. B. Y. Cotton
37. W. B. Cottrell
38. [illegible] S. Crouse
39. [illegible] L. Culler
40. [illegible] R. Cuneo
41. [illegible] H. DeVan
42. [illegible] M. Doney
43. D. A. Douglas
44. W. K. Eister
45. D. E. Ferguson
46. A. P. Fraas
47. J. H. Frye, Jr.
48. W. T. Furgerson
49. R. J. Gray
50. B. L. Greenstreet
51. A. T. Gresky
52. W. R. Grimes
53. A. G. Grindell
54. E. [illegible]th
55. C. [illegible] Harrill
56. E. [illegible]. Hoffman
57. [illegible] W. Hoffman
58. [illegible]. Hollaender
59. A. S. Householder
60. J. T. Howe
61. W. H. Jordan
62. P. R. Kasten
63. J. P. Kelly (K-25)
64. J. L. Kerrebrock
65. G. W. Keilholtz
66. C. P. Keim
67. F. L. Keller
68. M. T. Kelley
69. F. Kertesz
70. J. J. Keyes
71. P. G. Lafaytis
72. J. A. Lane
73. M. E. LaVerne
74. R. B. Lindauer
75. R. S. Livingston
76. R. N. Lyon
77. H. G. MacPherson
78. R. E. MacPherson
79. F. C. Maienschein
80. W. D. Manly
81. E. R. Mann
82. L. A. Mann
[illegible]. W. B. McDonald
84. J. R. McNally
85. [illegible]. R. McQuilkin
86. [illegible] V. Meghreblian
87. R. [illegible]. Milford
88. A. [illegible] Miller
89. R. E. Moore
90. J. G. Morgan
91. K. Z. Morgan
92. M. L. Nelson
93. G. J. Nessle
94. R. B. Ol[illegible]
95. L. [illegible]
96. P. Patriarca
97. S. K. Penny
98. A. M. Perry

99. D. Phillips
100. J. C. Pigg
101. A. E. Richt
102. M. W. Rosenthal
103. H. W. Savage
104. A. W. Sh[illegible]lainen
105. R. D. Sch[illegible]theiss
106. D. Scott
107. J. L. Scott
108. E. D. Shipley
109. A. Simon
110. O. Sisman
111. J. Sites
112. M. J. Skinner
113. A. H. Snell
114. F. J. Stanek
115. C. D. Susano
116. J. A. [illegible]wartout
117. J. [illegible] Tallackson
118. E. [illegible]. Taylor
119. [illegible] E. Thoma
120. [illegible]. B. Trauger
121. [illegible]D. K. Trubey
12[illegible] G. M. Watson
1[illegible]. A. M. Weinberg
[illegible]4. J. C. White
125. G. D. Whitman
126. E. P. Wigner (consultant)
127. J. C. Wilson
128. C. E. Winters
129. M. M. Yarosh
130. W. Zobel
131-133. ORNL - Y-12 Technical Library, Document Reference Section

[illegible]TERNA[illegible] DISTRIBUTION

134-136. Air Force Ballistic M[illegible]s[illegible]e Division
137-138. AFPR, Boeing, Seattle
139. AFPR, Boeing, Wichita
140. AFPR, Curtiss-Wright, [illegible]ton
141. AFPR, Douglas, Long [illegible]ach
142-144. AFPR, Douglas, Sant[illegible] Monic[illegible]
145. AFPR, Lockheed, Bu[illegible]ank
146-147. AFPR, Lockheed, M[illegible]ietta
148. AFPR, North Amer[illegible]an, Canoga [illegible]k
149. AFPR, North Ame[illegible]can, Downey
150-151. Air Force Spec[illegible]l Weapons Center
152. Air Materiel [illegible]mmand
153. Air Research [illegible]nd Development Comma[illegible] (RDGN)
154. Air Researc[illegible]and Development Comman[illegible] (RDTAPS)
155-168. Air Resear[illegible] and Development Command [illegible]DZPSP)
169. Air Techn[illegible]l Intelligence Center
170-172. ANP Proj[illegible]t Office, Fort Worth
173. Albuque[illegible]e Operations Office
174. Argonne [illegible]ational Laboratory
175. Armed [illegible]rces Special Weapons Project, Sandi[illegible]
176. Armed [illegible]rces Special Weapons Project, Washin[illegible]on
177. Assis[illegible]nt Secretary of the Air Force, R&D
178-183. Atom[illegible] Energy Commission, Washington
184. Ato[illegible]s International
185. Ba[illegible]lle Memorial Institute
186-187. Be[illegible]is Plant (WAPD)
188. Bureau of Aeronautics
189. Bureau of Aeronautics General Representative
190. BAR, Convair, San Diego
191. BAR, Aerojet-General, Azusa

192. BAR, Glenn L. Martin, Baltimore
193. BAR, Grumman Aircraft, Bethpage
194. Bureau of Yards and Docks
195. Chicago Operations Office
196. Chicago Patent Group
197. Curtiss-Wright Corporation
198. Engineer Research and Development Laboratories
199-202. General Electric Company (ANPD)
203. General Nuclear Engineering Corporation
204. Hartford Area Office
205. Idaho Operations Office
206. Knolls Atomic Power Laboratory
207. Lockland Area Office
208. Los Alamos Scientific Laboratory
209. Marquardt Aircraft Company
210. Martin Company
211. National Advisory Committee for Aeronautics, Cleveland
212. National Advisory Committee for Aeronautics, Washington
213. Naval Air Development Center
214. Naval Air Material Center
215. Naval Air Turbine Test Station
216. Naval Research Laboratory
217. New York Operations Office
218. Nuclear Development Corporation of America
219. Nuclear Metals, Inc.
220. Office of Naval Research
221. Office of the Chief of Naval Operations (OP-361)
222. Patent Branch, Washington
223-226. Pratt and Whitney Aircraft Division
227. San Francisco Operations Office
228. Sandia Corporation
229. School of Aviation Medicine
230. Sylvania-Corning Nuclear Corporation
231. Technical Research Group
232. USAF Headquarters
233. USAF Project Rand
234. U. S. Naval Radiological Defense Laboratory
235-236. University of California Radiation Laboratory, Livermore
237-254. Wright Air Development Center (WCOSI-3)
255-279. Technical Information Service Extension, Oak Ridge
280. Division of Research and Development, AEC, ORO

NOMENCLATURE

Na = sodium

Be = beryllium

G = energy deposition rate, watts per cubic centimeter

G' = energy deposition unit source, ^{o}F

α = fractional grid width for irregular boundary points

T = temperature, ^{o}F

$\underline{l}$ = dimensionless grid width

k = thermal conductivity, watts per inch per ^{o}F

h = film coefficient, watts per $inch^2$ per ^{o}F

γ_i = fraction of hole circumference

d = diameter of coolant holes, inches

∇^2 = Laplacian operator

q = heat, watts

R = radial location of inner and outer boundary of slab, inches

Z = vertical location of inner and outer boundary of slab, inches

ρ = radial coordinate, inches

t = thickness of slab, inches

[redacted]

TABLE OF CONTENTS

	Page
A. Introduction	4
1. Summary	4
2. The Reflector Moderator Cooling System	4
3. Gamma and Neutron Heat Deposition	5
4. Heat Transfer Model and Computational Procedure	5
B. The Relaxation Method	7
1. Two-Dimensional Temperature Distribution	7
2. Finite Difference Equation in Two Dimensions	7
3. Polar Transformation	9
4. Irregular Boundary Points	13
C. Heat Transfer Calculations	19
1. Subdivision of Reflector Into Slab Elements	19
2. Iteration Procedure	20
3. Boundary Temperatures Along Annuli	22
4. Total Heating in Beryllium	25
5. Holes That Do Not Encompass a Grid Point	26
D. Results	26
E. Appendix	30

[redacted]

INTRODUCTION

1. Summary. This report summarizes the application of the relaxation method to the determination of the steady state temperature distribution in the ART reflector beryllium during full power operation. The report includes a brief description of the reflector-moderator cooling system, the methods used in the calculations, and a summary of the results.

2. Reflector-Moderator Cooling System. A sketch of the reflector moderator cooling system is shown in Fig. 1. Cold sodium enters the top of the reflector and flows down through cooling holes in the beryllium and through the inner annulus. This sodium removes gamma and neutron heat deposited in the beryllium and also serves to cool the outer core shell. The flow then collects at the bottom of the reflector and passes up the outer annulus, removing heat from the shell structure beyond the reflector.

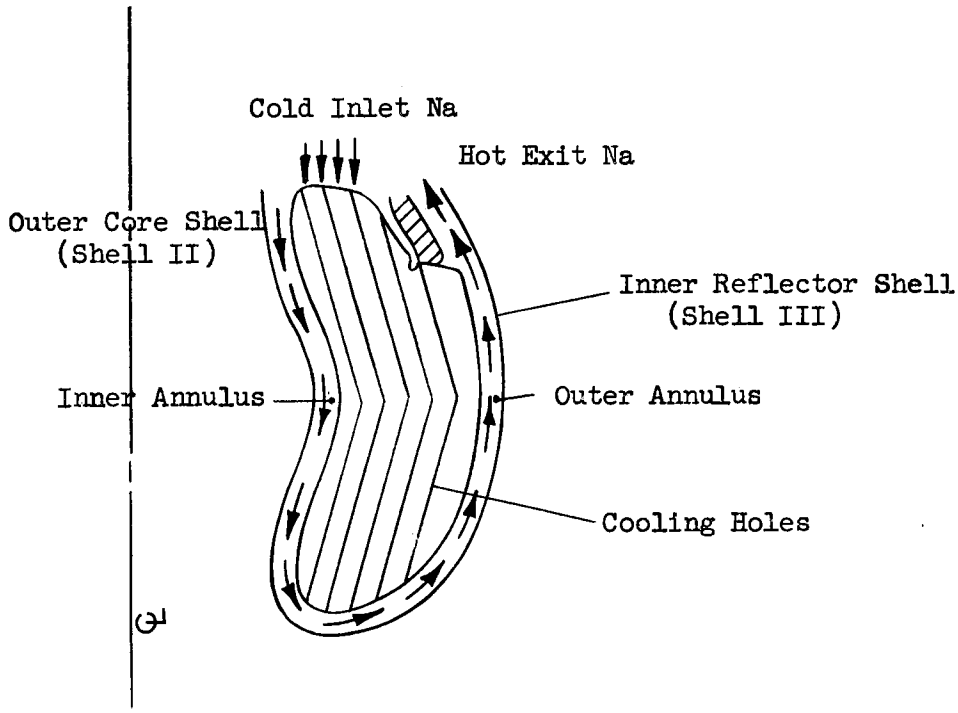

Fig. 1 Reflector-Moderator Cooling System

For a particular sodium flow rate and flow distribution among the various cooling passages, a steady state temperature distribution exists throughout the beryllium during full power operation. The purpose of this study is to determine that temperature distribution.

3. Gamma and Neutron Heat Deposition. Gamma sources were based in part on computed fluxes. These sources were produced by radiative capture and inelastic scattering. Other gamma sources were determined from the measured flux levels in the hot critical experiment. The gamma ray energy deposition rates were then calculated by means of the buildup factor technique, using a program designed by Pratt and Whitney for the IBM 704[1]. The neutron heating was computed from the two-dimensional multigroup flux calculation.

4. Heat Transfer Model and Computational Procedures. The determination of the temperature distribution required the solution of a three-dimensional heat conduction problem with non-uniform internal heat generation. As a further complication, the fluid boundary temperatures were dependent upon the heat transferred between the solid and the fluid, and hence, upon the integrated heat fluxes at the boundaries. In terms of the reflector-moderator cooling system, the rise in sodium temperature as it flows through each cooling hole and annulus is dependent upon the heat flux at the surface of the beryllium, which in turn is dependent upon the local sodium temperature.

It was apparent from the complicated geometry and spacial heating distribution that an analytical solution would be totally impractical. Certain simplifying features, however, made possible a numerical solution which was reduced to a series of two dimensional problems. These were solved with the aid of an IBM-650.

Because of axial symmetry in the cooling hole pattern it was necessary to solve for the temperature distribution in only one segment of the reflector, resembling an "orange slice". The cooling hole pattern repeats every 5-degrees of azimuth. A sketch of the orange slice and a typical cross-section through the slice is shown in Fig. 2. The vertical faces of the slice were considered to be insulated for the calculations.

---

1. H. W. Bertini, C. M. Copenhaver, A. M. Perry, R. B. Stevenson, Basic Gamma Ray Data for ART Heat Deposition Calculations, ORNL 2113.

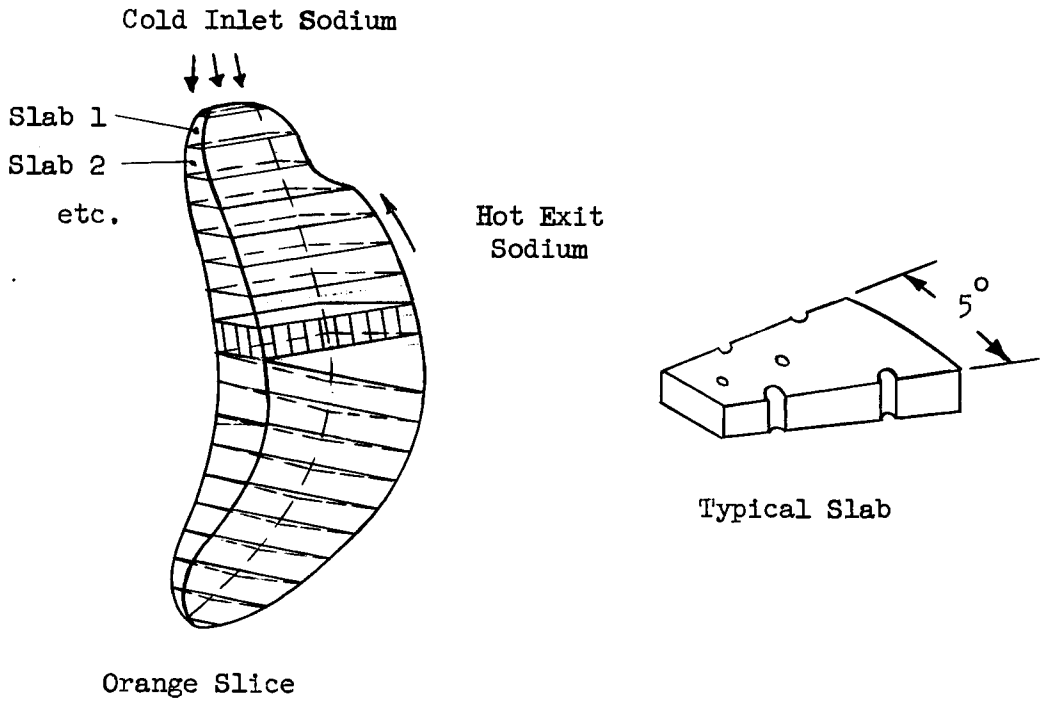

Fig. 2 Orange Slice Showing Cuts Perpendicular to Cooling Holes and Typical Slab

Since the sodium temperatures in the inner and outer annuli are primarily determined by the heat fluxes from the adjacent shells, it was possible to obtain initial estimates of these temperatures independent of the beryllium temperature distribution. These temperature distributions served to establish the boundary conditions on the inner and outer surfaces of the beryllium[2,3].

---

2. R. I. Gray, Proposed Report on ART Sodium Coolant System.

3. H. W. Hoffman, C. M. Copenhaver, J. L. Wantland, Thermal Structure for the Region Beyond the ART Reflector, ORNL CF 56-3-23 Supplement I - ORNL CF 56-4-129.

With a knowledge of the boundary conditions for the inner and outer edges and the two insulated faces of the orange slice, the remaining problem was to determine the temperature structure throughout the beryllium and the sodium in the cooling holes. Since the heat flow is primarily in a direction perpendicular to the holes, it was possible to reduce the three dimensional problem to a series of two dimensional problems by treating further slices of the orange slice with cuts perpendicular to the holes. By assuming the faces of each slab to be insulated, the two dimensional temperature distribution could be determined for a given set of cooling hole temperatures. From this temperature distribution, and the sodium flow rate for each hole, the heat load to the various holes and the temperature rises for the next slab could be calculated.

The orange slice was divided into 23 slabs as illustrated in Fig. 2. Starting with Slab 1, the sodium temperatures for the various holes were taken uniformly as the inlet sodium temperature. From the two-dimensional temperature distribution calculated for this slab and the sodium flow rates for each hole, the heat loads to the holes and the temperature rises were calculated, establishing the boundary conditions for Slab 2. This process was repeated until the entire temperature distribution was obtained. The temperature of the sodium leaving the coolant passages at the bottom of the reflector should be within a few degrees of the assumed inner annulus temperature at that point. The agreement here was very close.

RELAXATION METHOD

1. Two-Dimensional Temperature Distribution. A numerical method was used to solve for the two-dimensional temperature distribution in each slab. With the aid of a polar transformation to convert the cross-section of Fig. 2 into a rectangular shape, a square grid was used to approximate the heat conduction equation by finite differences. The set of finite-difference equations for each slab was solved on an IBM-650 using a Gauss-Seidel technique.

2. Finite Difference Equation in Two Dimensions. The heat conduction equation with internal heat generation is given by

$$\nabla^2 T(x,y) + \frac{G(x,y)}{k} = 0 \qquad (1)$$

where ∇^2 is the Laplacian operator, x and y are the cartesian coordinates, T is the temperature, G is the heat generation rate and k is the thermal conductivity.

For a square grid, of grid width, $\underline{l}$, using the nomenclature of Fig. 3, the finite-difference approximation to Eq. (1) may be obtained for point T_o, as follows:

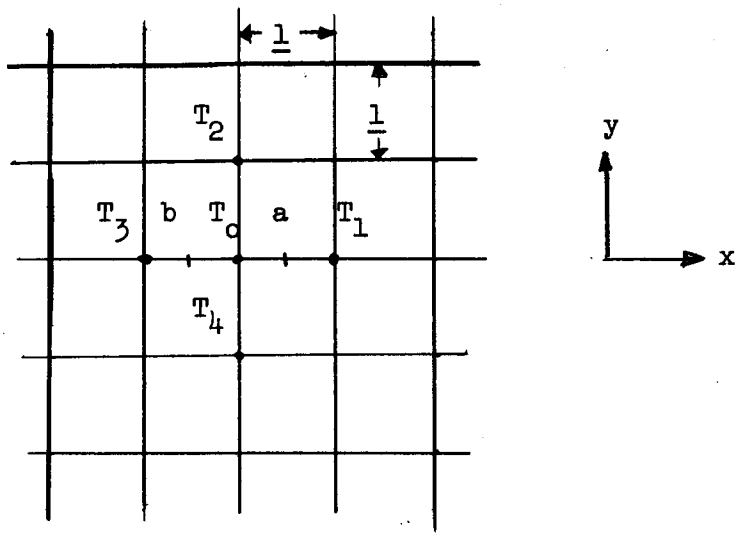

Fig. 3 Square Grid in Cartesian Coordinates

The first partial derivatives with respect to x at points a and b may be approximated by

$$\left(\frac{\partial T}{\partial x}\right)_a = \frac{T_1 - T_o}{\Delta x} = \frac{T_1 - T_o}{\underline{l}} \tag{2}$$

$$\left(\frac{\partial T}{\partial x}\right)_b = \frac{T_o - T_3}{\Delta x} = \frac{T_o - T_3}{\underline{l}} \tag{3}$$

The second partial derivative with respect to x at T_o may be approximated by,

$$\left(\frac{\partial^2 T}{\partial x^2}\right)_o = \frac{\left(\frac{\partial T}{\partial x}\right)_a - \left(\frac{\partial T}{\partial x}\right)_b}{\Delta x} = \frac{T_1 + T_3 - 2T_o}{\underline{l}^2} \tag{4}$$

Similarly,

$$\left(\frac{\partial^2 T}{\partial y^2}\right)_o = \frac{T_2 + T_4 - 2T_o}{\underline{l}^2} \tag{5}$$

Substituting (4) and (5) into (1),

$$T_1 + T_2 + T_3 + T_4 - 4T_o + \frac{\underline{l}^2 G(x,y)}{k} = 0 \tag{6}$$

Equation (6) is the usual finite difference equation to be satisfied at each internal point in the grid. The equations for treating boundary points are discussed in subsequent sections.

3. Polar Transformation. If the cross-section of Fig. 2 were to be approximated by a square grid, almost all of the boundary points would be irregular. In other words, the points representing the boundary of the solid would not lie on regular mesh points in the grid. This would require a particular finite difference equation, in general more complicated than Eq. (6), for a large number of points. This complication was avoided by transforming the cross-section of Fig. 2 into a rectangle through the use of a polar transformation. The rectangle was simply handled by the square grid and required few irregular points. However, the finite difference equation corresponding to Eq. (6) had to be modified slightly.

The polar coordinates, ρ and θ, may be transformed to cartesian coordinates, u and v, by the relations,

$$u = \ln \rho \tag{7}$$

$$v = \theta \tag{8}$$

The transformation of the cylindrical-segment of Fig. 2 to a rectangle is illustrated in Fig. 4.

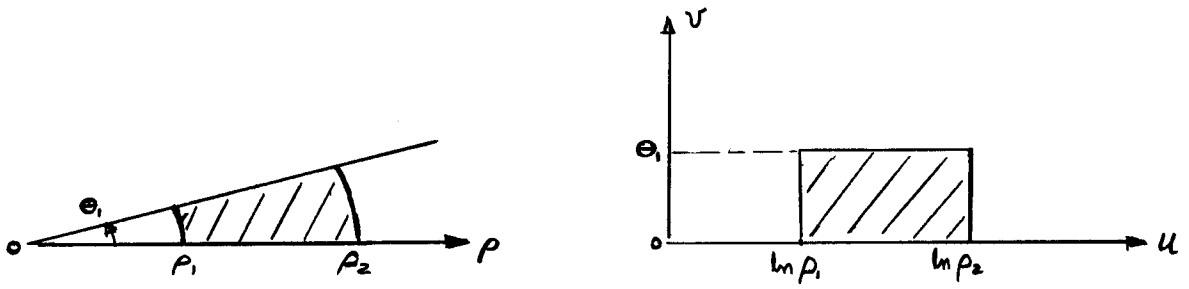

Fig. 4 Polar Transformation of Cylindrical Segment to Rectangle

Rewriting Eq. (1) in polar coordinates,

$$\frac{\partial^2 T(\rho,\theta)}{\partial \rho^2} + \frac{1}{\rho}\frac{\partial T(\rho,\theta)}{\partial \rho} + \frac{1}{\rho^2}\frac{\partial^2 T(\rho,\theta)}{\partial \theta^2} + \frac{G(\rho,\theta)}{k} = 0 \tag{9}$$

By changing variables according to Equations (7) and (8),

$$\nabla^2_{\rho,\theta} = \frac{1}{\rho^2}\left(\frac{\partial^2}{\partial u^2} + \frac{\partial^2}{\partial v^2}\right) = \frac{1}{\rho^2}\nabla^2_{u,v} \tag{10}$$

The application of Eq. (10) to Eq. (9) yields

$$\nabla^2 T(u,v) + \frac{\rho^2 G}{k} = 0 \tag{11}$$

Due to symmetry the heat deposition rate is a function of ρ, and therefore u, only; thus,

$$\nabla^2 T(u,v) + \frac{\rho^2 G(u)}{k} = 0 \tag{12}$$

The finite difference equation may now be written for Eq. (12) by taking a square grid with

$$\underline{1} = \Delta u = \Delta v = \Delta \theta \tag{13}$$

Constructing the partial derivatives as before, the finite difference equation corresponding to Eq. (6) becomes

$$T_1 + T_2 + T_3 + T_4 - 4T_o + \frac{\rho^2 \underline{1}^2 G(\rho)}{k} = 0 \tag{14}$$

Note that there is now a ρ^2 in the source term for each mesh point in the grid. This added computation required in preparing each problem for the machine calculations was more than compensated for by the reduction in the number of irregular points for each grid.

A grid width was selected which divided the angular width of the slab into six equal parts. By using a square grid of this width, irregular points were required only for the inner and outer edges of the slabs and for the cooling holes. The total number of points in the grid for each slab ranged from about 300 to 450, of which about 25 to 35 were irregular. Fig. 5 shows a typical grid in both the transformed and untransformed planes. The irregular points are shown in the transformed section.

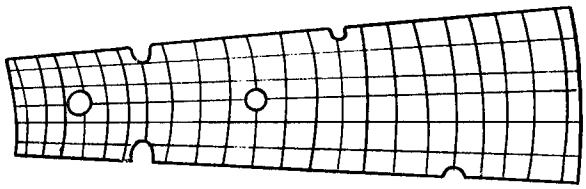

Untransformed Grid in ρ,θ - plane

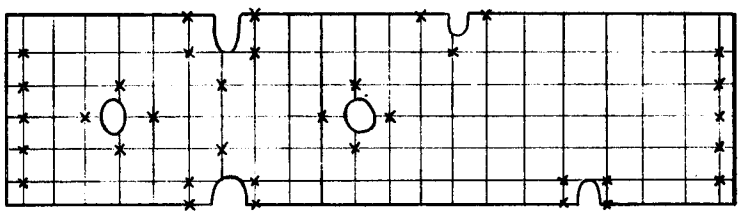

Transformed Grid in u,v - plane
(Irregular points are starred.)

Fig. 5 Square Grid in Transformed Plane Showing Transformed and Untransformed Cross-Sections

4. Irregular Boundary Points. A general coefficient was derived for a point adjacent to a fluid boundary, at which heat transfer to the fluid is described in terms of a heat transfer coefficient. The finite-difference equation was derived by taking a second order power series expansion of the temperature function about the point adjacent to the boundary.

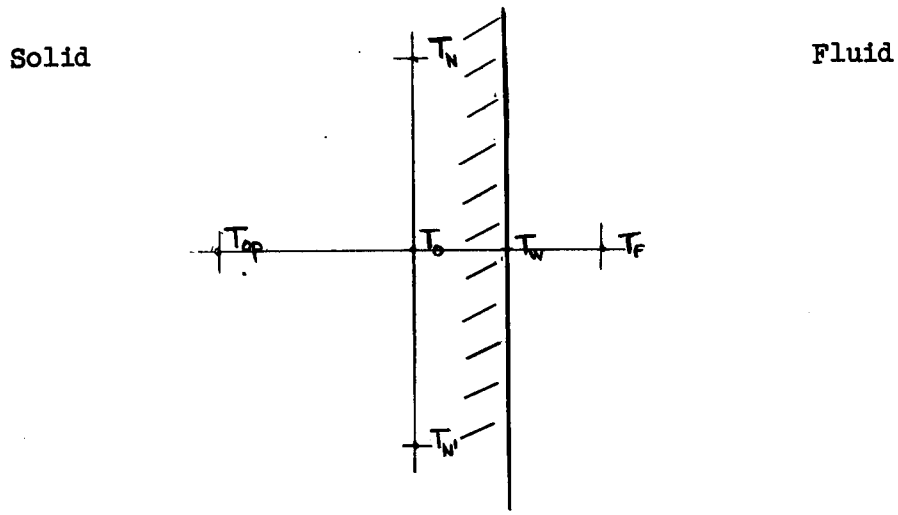

Fig. 6 Typical Boundary Point

Fig. 6 shows a typical boundary point, T_o, a fractional grid distance, α, from the boundary. The symbols, T_w and T_f denote the wall and fluid temperatures. A finite difference equation is required expressing T_o in terms of the surrounding points T_f, T_N, $T_{N'}$, and T_{op}. Although T_f does not represent a true grid point, it is treated as a grid point for the calculations, and its value is held constant at the appropriate fluid temperature. The temperature, T_{op}, is a regular internal point, for which Eq. (14) is applicable.

If the origin for the x axis is taken at T_o, and the temperature function is expanded about the point zero, then

$$T(x) = T_o + a_1 x + a_2 x^2 \tag{15}$$

The application of this relation to the temperature at $x = \alpha \underline{l}$ and $x = -\underline{l}$ yields:

$$T_w = T_o + a_1 \alpha \underline{l} + a_2 (\alpha \underline{l})^2 \tag{16}$$

$$T_{op} = T_o - a_1 \underline{l} + a_2 \underline{l}^2 \tag{17}$$

By equating the heat flux at the wall to the heat transferred to the fluid from the wall, we have

$$- k \left[\frac{\partial T}{\partial x}\right]_{x=\alpha \underline{l}} = h(T_w - T_f) \tag{18}$$

But, from Eq. (15),

$$\left[\frac{\partial T}{\partial x}\right]_{x=\alpha \underline{l}} = \left[a_1 + 2a_2 x\right]_{x=\alpha \underline{l}} = a_1 + 2a_2 \underline{l} \tag{19}$$

The substitution of Eq. (18) into Eq. (19) gives

$$- k (a_1 + 2a_2 \alpha \underline{l}) = h(T_w - T_f) \tag{20}$$

By the application of Eqs. (16), (17), and (20), an expression can be obtained for T_w in terms of T_o, T_{op}, and T_f; the result is,

$$T_w = \frac{T_f + \frac{h\underline{l}\alpha}{k} + T_o(1+\alpha) - T_{op}\frac{\alpha^2}{1+\alpha}}{\frac{1+2\alpha}{1+\alpha} + \frac{h\underline{l}\alpha}{k}} \tag{21}$$

The finite-difference equation for T_o in cartesian coordinates may now be derived by taking a heat balance on an element of volume around T_o, and replacing T_w by its value from Eq. (21). Unit thickness is assumed for the slab, and the resultant heat balance may be expressed by

$$K(T_N + T_N' + T_{op} - 3T_o) + h\underline{l}(T_f - T_w) + \underline{l}^2 G(x_o, y_o) = 0 \tag{22}$$

Substituting T_w from Eq. (21) into Eq. (22),

$$C_f T_f + T_N + C_{op} T_{op} + T_{N'} - C_o T_o + \frac{\underline{l}^2 G(x_o, y_o)}{k} = 0 \tag{23}$$

where,

$$C_f = \frac{h\underline{l}}{k} - \frac{\left(\frac{h}{k}\right)^2 \underline{l}^2 \alpha}{\frac{1+2\alpha}{1+\alpha} + \frac{h\underline{l}\alpha}{k}} \tag{23a}$$

$$C_{op} = 1 + \frac{\frac{h\underline{l}}{k} + \frac{\alpha^2}{(1+\alpha)}}{\frac{1+2\alpha}{1+\alpha} + \frac{h\underline{l}\alpha}{k}} \tag{23b}$$

$$C_o = 3 + \frac{\frac{h\underline{l}}{k}(1+\alpha)}{\frac{1+2\alpha}{1+\alpha} + \frac{h\underline{l}\alpha}{k}} \tag{23c}$$

Equation (23) is the finite-difference equation corresponding to Eq. (6). This can be modified for use with the polar transformation by replacing the heat transfer length, $\underline{l}$ in Eqs. (21) and (22) by $\rho\underline{l}$, the approximate corresponding length in the untransformed polar plane. Note that this substitution gives Eq. (14) directly from Eq. (6). Again, since the heat deposition rate is a function of ρ only, $G(x_o,y_o)$ can be replaced by $G(\rho_o)$. The resulting equation is

$$C_f T_f + T_N + C_{op} T_{op} + T_{N'} - C_o T_o + \frac{\rho^2 \underline{l}^2 G(\rho_o)}{k} = 0 \quad , \tag{24}$$

where

$$C_f = \frac{h\rho\underline{l}}{k} - \frac{\left(\frac{h}{k}\right)^2 \rho^2 \underline{l}^2 \alpha}{\left[\frac{1+2\alpha}{1+\alpha} + \frac{h\rho\underline{l}\alpha}{k}\right]} \tag{24a}$$

$$C_{op} = 1 + \frac{\frac{h\rho\underline{l}}{k} \cdot \frac{\alpha^2}{1+\alpha}}{\left[\frac{1+2\alpha}{1+\alpha} + \frac{h\rho\underline{l}\alpha}{k}\right]} \tag{24b}$$

$$C_o = 3 + \frac{\frac{h\rho\underline{l}}{k}(1+\alpha)}{\left[\frac{1+2\alpha}{1+\alpha} + \frac{h\rho\underline{l}\alpha}{k}\right]} \tag{24c}$$

Equation (24) was used for points along the inner and outer edges of the slab. For points adjacent to the holes the equation was modified to account for the actual surface area of the volume element in contact with the fluid. Since the dimension of the holes is very small in comparison to the radial variable, ρ, the holes remain approximately circular in the transformed plane. If πd is the actual circumference of the hole in the untransformed plane, $\pi d/\rho$ is the approximate circumference in the transformed plane, where ρ is the

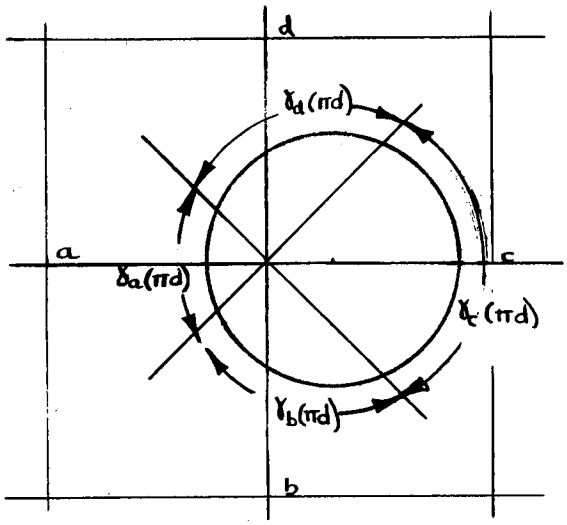

Fig. 7 Irregular Points Adjacent to Hole

radial distance to the hole. To modify Eq. (24) for points as shown in Fig. 7, the heat transfer area, $\underline{1}$, associated with the fluid heat transfer terms in Eqs. (21) and (22), was replaced by $\gamma_i(\pi d)$. As shown in Fig. 7, γ_i represents the fraction of the circumference over which heat is transferred to the fluid from the i th point adjacent to the hole.

Making these substitutions,

$$C_f T_f + T_N + C_{op} T_{op} + T_{N'} - C_o T_o + \frac{\rho^2 \underline{1}^2 G(\rho_o)}{k} = 0 \tag{25}$$

where,

$$C_f = \frac{h\gamma_o \pi d}{k} - \frac{\left(\frac{h}{k}\right)^2 (\gamma_o \pi d)^2 \alpha}{\left[\frac{1+2\alpha}{1+\alpha} + \frac{h\gamma_o \pi d \alpha}{k}\right]} \tag{25a}$$

$$C_{op} = 1 + \frac{\left(\frac{h\gamma_o \pi d}{k}\right) \frac{\alpha^2}{1+\alpha}}{\left[\frac{1+2\alpha}{1+\alpha} + \frac{h\gamma_o \pi d \alpha}{k}\right]} \tag{25b}$$

$$C_o = 3 + \frac{\left(\frac{h\gamma_o \pi d}{k}\right)(1+\alpha)}{\left[\frac{1+2\alpha}{1+\alpha} + \frac{h\gamma_o \pi d \alpha}{k}\right]} \tag{25c}$$

HEAT TRANSFER CALCULATIONS

1. Subdivision of Reflector Into Slab Elements. The following system of nomenclature will be used:

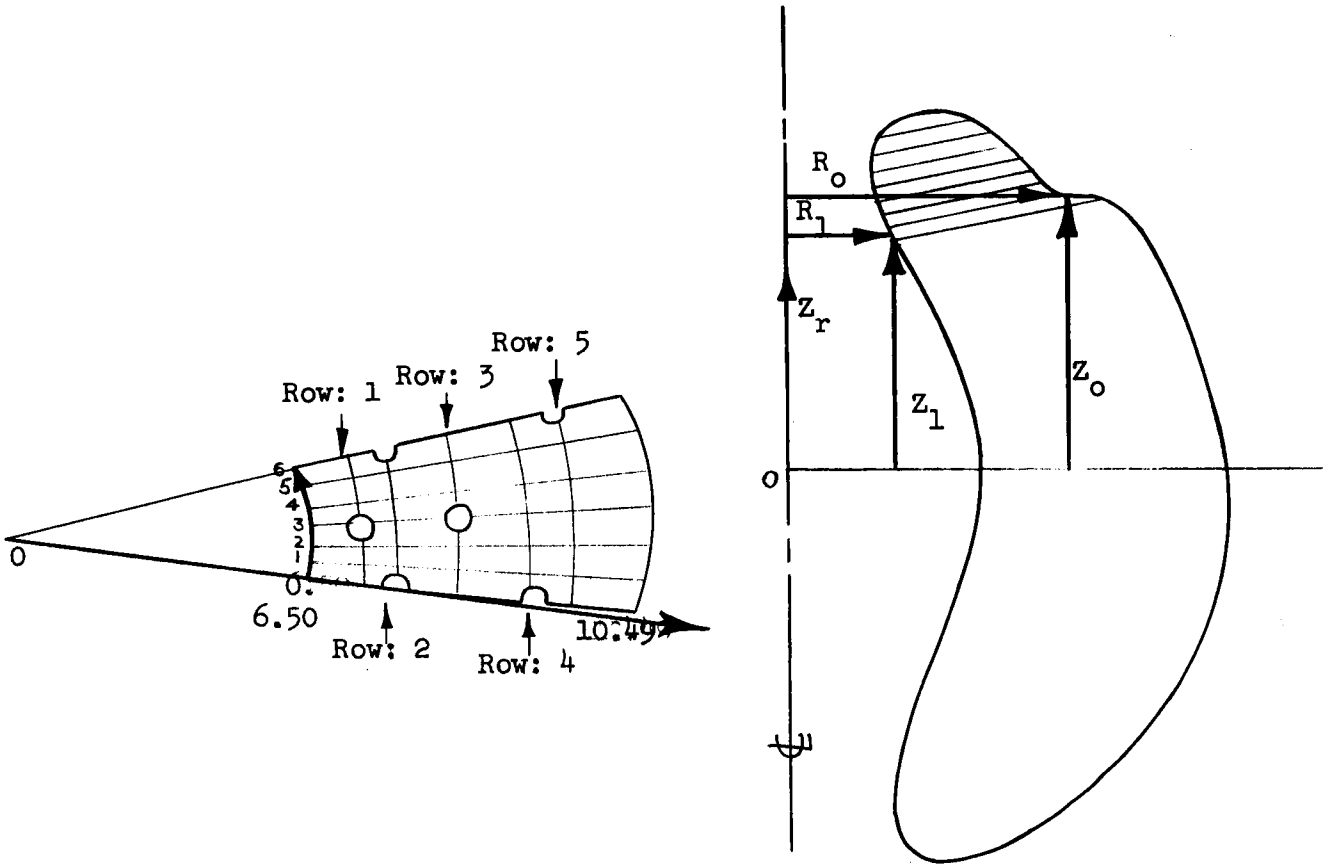

(a) (b)

Fig. 8 Nomenclature of Slabs

All slabs except 1, 11, 22 are 1.75" thick. Slab 1 is 1" thick, slab 11 is a wedge with variable thickness, and slab 22 is 0.75" thick. The numbering of the slabs runs from the top of the Be reflector to the bottom. All slabs except 11 are inclined 15° to the equator. In this manner the slabs will be perpendicular to the cooling passages. The radial distance ρ is always measured from the true axis. A 5° cut of the total reflector is always used in the solution of the problem. This 5° will be subdivided into six parts as shown by the j

coordinate. Figure 8(a) shows a typical slab in which all five holes appear, although there are some slabs in which the slab does not extend beyond the third or fourth hole. The position of each slab as shown in Fig. 8(b) may be found in Appendix I.

2. Iteration Procedure. After the temperature profile for any slab is obtained, the heat rejected to any hole can be calculated by the use of the gradient through the boundary points. From the heat balance at a boundary point to a hole (see Figs. 6 and 7)

$$(T_{op} - T_o) + (T_N - T_o) + (T_{N'} - T_o) + \frac{h}{k}(T_f - T_w)\gamma_i \pi d + G' = 0 \qquad (26)$$

which is to be compared to Eq. (22). Let q' be the heat passed to the sodium through the boundary $\gamma_i \pi d$, that is,

$$q' = \frac{h}{k}(T_f - T_w)\gamma_i \pi d \qquad (27)$$

where q' has the units of temperature. This relation is used in Eq. (26); thus we obtain

$$q' = T_{op} + T_N + T_{N'} + G' - 3T_o \qquad (28)$$

The actual heat passed through the boundary, $\gamma_i \pi d$, of a slab of thickness t is computed from

$$q(\text{watts}) = q'(^{o}F) \cdot k(\text{watts/cm}^{o}F) \cdot t(\text{cm}) \qquad (28a)$$

The factor kt will vary from slab to slab, and in slab 11, it will also vary from hole to hole.

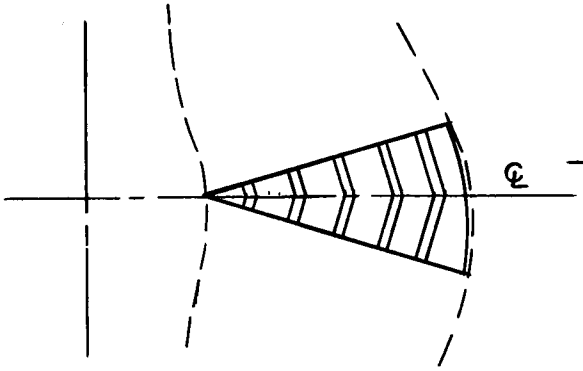

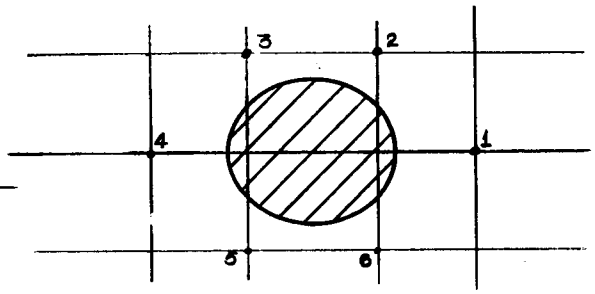

Fig. 9 Slab 11 (at equator) Fig. 10 Heat Summation Around Hole

In this case, the thickness will vary and an average thickness for each hole will be used.

The q values obtained from Eq. (28a) are summed about the hole until all boundary points are considered. For example, in the case of the point shown in Fig. 10, the total heat taken up may be written in the form

$$q_{Total} = q_{①} + q_{②} + q_{③} + q_{④} + q_{⑤} + q_{⑥} \tag{29}$$

The temperature rise in the sodium as it passes through the slab may be calculated from the following relationship,

$$q = WC_p\Delta T \tag{30}$$

where q is expressed in the units, BTU/hr; W in the units, lb/hr; ΔT, ^{o}F; and C_p in the units BTU/lb ^{o}F. This heat capacity symbol, C_p, is assumed to be constant throughout the temperature range of this problem and to have a value of 0.3. The flow rates, W, for the various holes, were set by a preliminary investigation of the heat distribution and are listed in Appendix V. In the case of the nth slab,

[redacted]

[redacted]

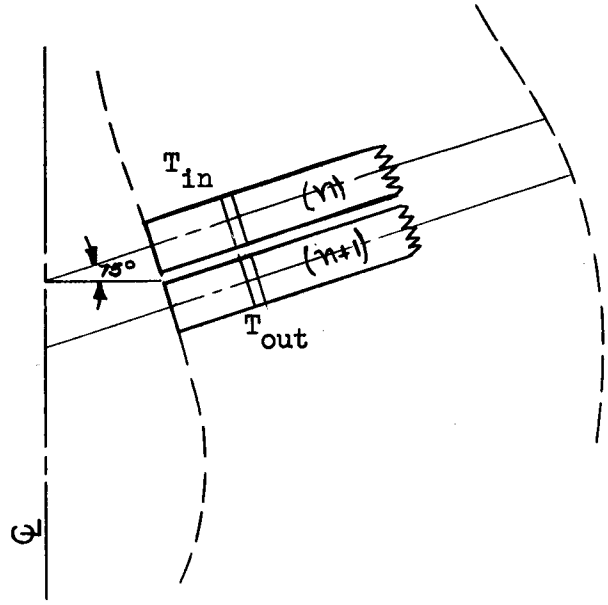

Fig. 11 Slab Iteration

$$T_{out}(n) = T_{in}(n) + \Delta T(n), \text{ and} \tag{31}$$

$$T_{in}(n+1) = T_{out}(n) \tag{31a}$$

The heat deposited to each hole and the temperatures, $T_{in}(n+1)$, calculated from this heat are given in Appendix V.

Since the temperatures of the sodium in the inner and outer annulus have already been set, all boundary conditions for the slab are now known.

3. Boundary Temperatures Along Annuli. The sodium temperature rise in the inner annulus is dependent to a large degree on the core heat rejected through shell II. It had previously been assumed that the Be would furnish 9 percent of this rise. With the design flow rate, the rise in the temperature due to Be heating alone would be 12°F. This flow rate was checked by actually computing the heat transferred across the inner boundary after the first complete iteration through the 23 slabs had been completed. Consider the point, T_o, shown in Fig. 12.

[redacted]

[redacted]

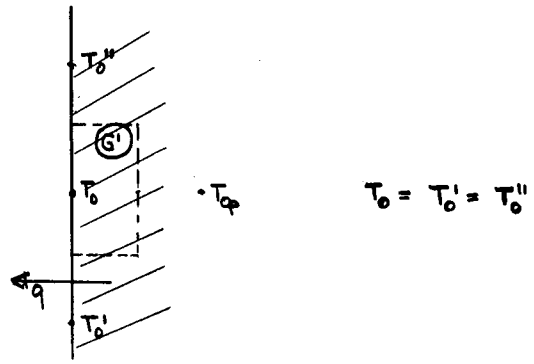

Fig. 12 Inner Boundary

Here:

$$q(\text{watts}/5^{\circ}\text{slab}) = (T_{op}-T_o+G')\ {}^{\circ}\text{F}\cdot(\text{kt})\ \text{watts}/{}^{\circ}\text{F}\cdot(6)\text{grid pts./slab} \qquad (32)$$

Then,

$$q_{\text{refl.}}(\text{watts}) = 72 \sum_{1}^{23} q(\text{watts}/5^{\circ}\text{slab}) \qquad (33)$$

and from Eq. (30), the sodium temperature rise in the inner annulus may be determined. These computations and results are given in Appendix II. It was found that the temperature rise was 13.4°F, which agrees favorably with the design flow rate.

The outer annulus temperature depends on heat received from the main heat exchangers. There is very slight temperature rise in this return coolant due to Be heating. This temperature is 1205°F at the lower header and 1250°F at the upper header.

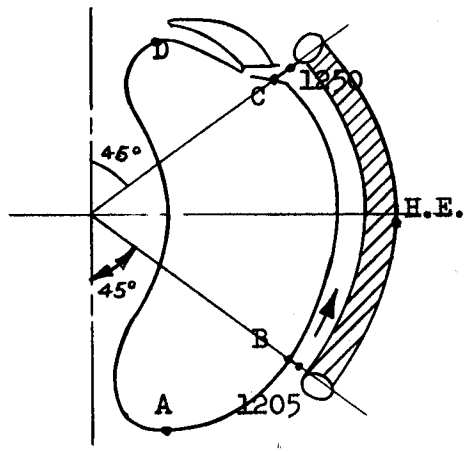

Fig. 13 Outer Boundary

The temperatures from B to A cannot be set until the iteration process has proceeded to point B. Then from consideration of the sodium temperatures at that point, good assumptions can be made. At point C, the return sodium leaves the Be and flows around the support ring. The outer boundary from D to C is actually dependent on the inlet sodium. In this region, the temperature of the sodium progressively rises due to the following effects:

(i) Heating within Inconel support ring and boron steel plates
(ii) Heating within boron copper cone
(iii) Conduction of heat from 1250°F return sodium.

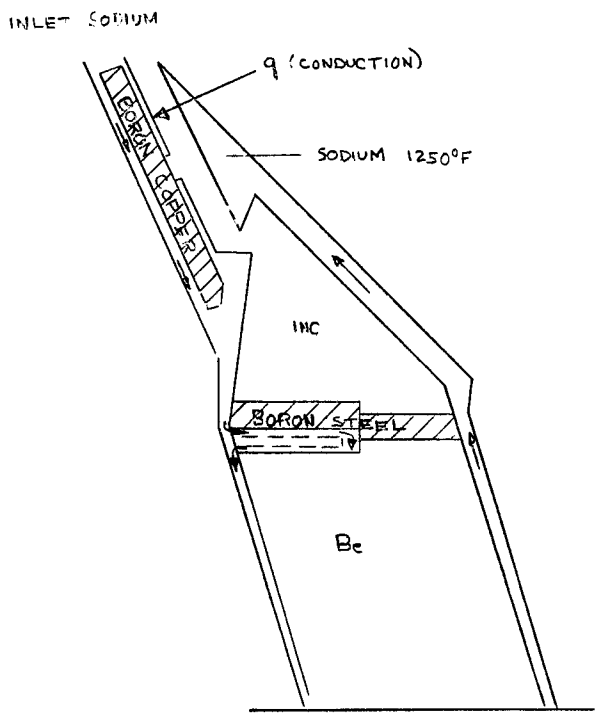

Fig. 14 External Sources of Heat to Inlet Na

The heat acquired from these effects results in a temperature rise of 90°F in the outer row of holes. This is the temperature which enters slab 6; thus, (see Appendix VI) the temperature of the sodium entering slab 6 is equal to the inlet sodium temperature, plus the ΔT (external sources), plus ΔT (internal heat generated within the Be). Or,

$$T_{Na}(\text{slab } 6) = 1050^{\circ}F + 90^{\circ}F + \Delta T(\text{internal}) \tag{34}$$

4. Total Heating in Be. An essential step in the determination of the sodium flow rates in the reflector was the computation of the heat rejected to the various coolant passages. This information was obtained by graphically integrating the total heating within the reflector. In the present analysis, the heat picked up by the sodium is obtained by summing the contributions from individual slabs. In this calculation, all surfaces of equal heating rate were considered to be perpendicular to the slab and to have the value at the center of the slab. Thus in Fig. 15,

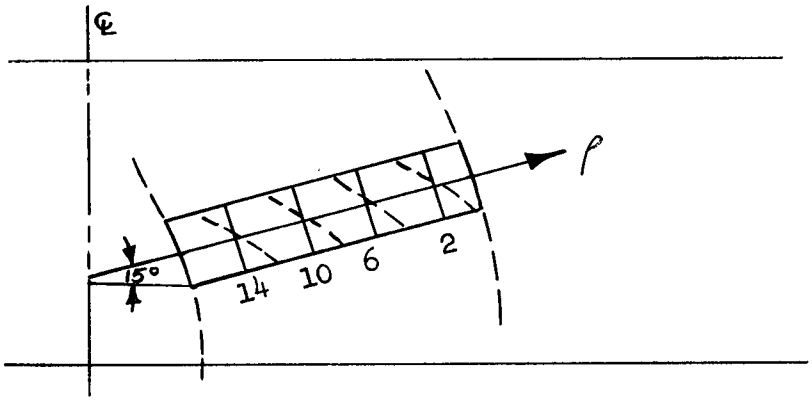

Fig. 15 Energy Deposition Rates in Typical Slab

The broken lines are the contours of the actual heating rate and the solid lines are their necessary approximations. By this approximation a graph of the energy deposition rate was plotted as a function of a radial coordinate, ρ. Thus,

$$G' = \frac{\rho^2 \underline{l}^2 G}{\bar{k}} \tag{35}$$

where $\underline{l}$ is the transformed grid width. This relationship converts the heating rate given in the cylindrical coordinates to the transformed square grid. The source term, G', is in units of °F and refers to the unit heat generation about each grid point. These values of G' can then be summed throughout the entire reflector. In this manner, the total amount of heat, as obtained by the previously mentioned approximation, could be compared to the results from the graphical integration (see Appendix III). It should be noted that these individual unit sources of heat made up the problem that was actually solved in the temperature solution of the reflector.

By previous graphical integration	By geometric approximation and transformation
q = 1.55 megawatts	q = 1.58 megawatts

The agreement is very good.

5. Holes That Do Not Encompass a Grid Point. The following difficulty arose on numerous instances.

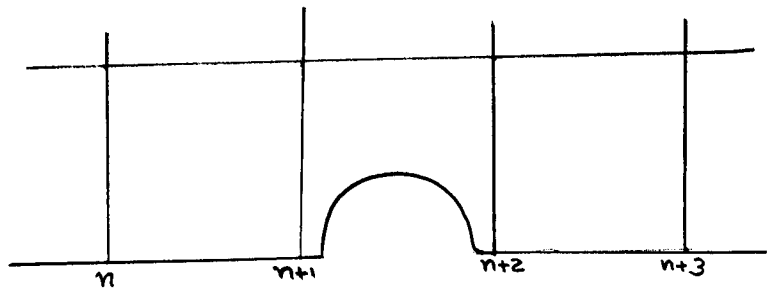

Fig. 16 Holes That Do Not Encompass a Grid Point

Here the true physical significance cannot be stated by the customary heat balance, Eq. (23), since there is no grid point to represent T_f although boundary points, n+1 and n+2, both reject heat through a finite heat transfer area into a coolant passage. This problem was solved by setting $T_f = 0$ and adding the heat into the external heat source term. Thus,

$$C_n T_n + C_{n'} T_{n'} + C_{op} T_{op} + G'' - C_o T_o = 0 \tag{36}$$

where G" is equal to G'(unit heat) plus $C_f T_f$. No difficulty was experienced using this method.

RESULTS

Temperature profiles are given in this section for three representative slabs. These slabs are: slab 6 which is immediately below the support ring, slab 11 which is at the equator, and slab 20 where row five exits into the return annulus. The temperatures at the various (i,j) points for each slab, along with their corresponding ρ distance, are given in Appendix VII.

ORNL-LR-DWG. 27095

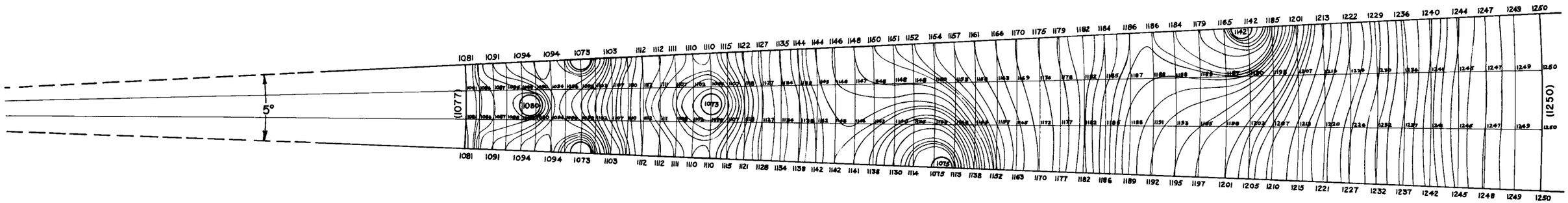

TEMPERATURE PROFILE OF SLAB-6

SCALE~2=1

[redacted]

ORNL-LR-DWG. 27093

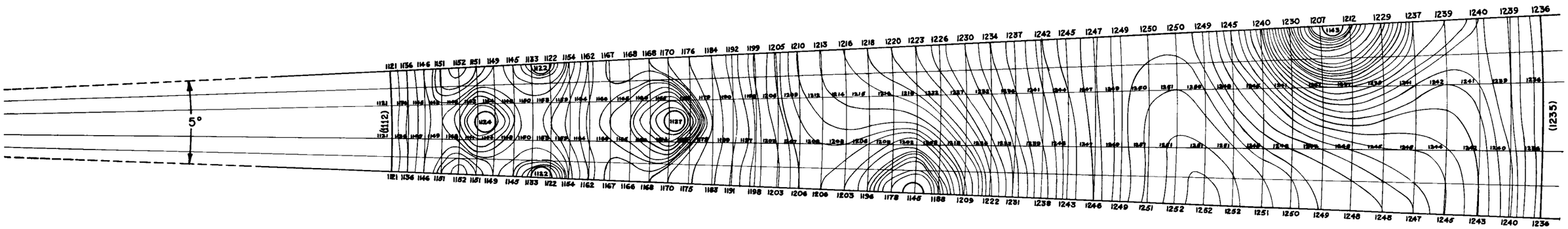

TEMPERATURE PROFILE OF SLAB-II

SCALE ~ 2=1

[redacted]

ORNL-LR-DWG. 27094

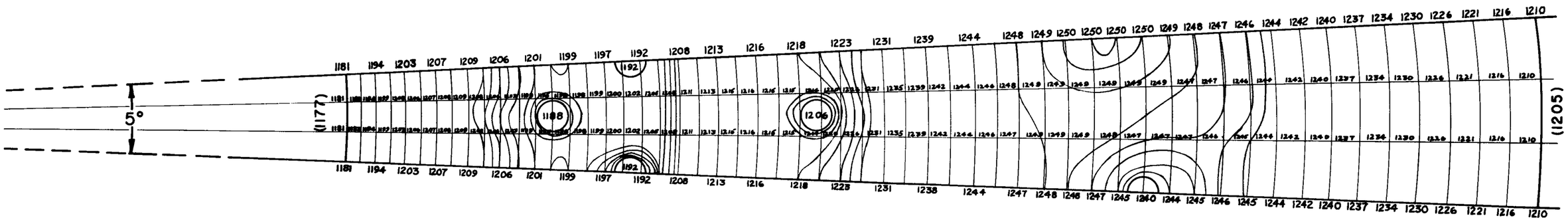

TEMPERATURE PROFILE OF SLAB-20

SCALE—2:1

[redacted]

[redacted]

Appendix I

Basic Slab Data

Slab	R_1-in	R_o-in	Z_1-in	Z_o-in	Temp-°F inside annulus	Temp-°F outside annulus
1	1.8720	2.3560	15.45	16.45	1050	1050
2	1.9210	2.5470	14.05	15.60	1058	1050
3	2.0000	2.6430	12.40	14.15	1061	1080
4	2.0820	2.7190	10.75	12.60	1067	1110
5	2.1630	2.7700	9.25	10.95	1072	1140
6	2.2390	2.9860	7.65	10.10	1077	1250
7	2.3100	3.0020	6.00	8.60	1082	1246
8	2.3620	3.0190	4.30	7.00	1090	1244
9	2.3400	3.0810	2.65	5.35	1098	1241
10	2.4130	3.0990	0.90	3.70	1105	1238
11	2.3890	3.0860	0.00	0.00	1112	1235
12	2.4130	3.0990	-0.90	-3.70	1117	1231
13	2.3400	3.0810	-2.65	-5.35	1125	1227
14	2.3620	3.0190	-4.30	-7.00	1135	1223
15	2.3100	3.0020	-6.00	-8.60	1143	1219
16	2.2390	2.9860	-7.65	-10.10	1151	1216
17	2.1630	2.9370	-9.65	-10.95	1158	1213
18	2.0820	2.875	-10.75	-12.60	1166	1210
19	2.0000	2.8000	-12.40	-14.70	1171	1207
20	1.9210	2.7900	-14.05	-16.10	1177	1205
21	1.8560	2.5650	-15.95	-17.55	1183	1205
22	1.8900	2.4620	-17.20	-18.40	1185	1202
23	1.8410	2.3030	-18.35	-19.20	1189	1199

[redacted]

[redacted]

[redacted]

[redacted]

Appendix II

Heat Rejected Into Inner Na Annulus

Slab	kt / w/°F	T_{op} / °F	4K / °F	T_o / °F	$(T_{op}+K'-T_o)$ / °F	q / watts
1	1.397	57.095	.400	53.091	4.404	5.924
2	2.4003	67.304	.528	61.683	6.149	14.759
3	2.4003	73.081	.916	65.642	8.355	20.054
4	2.4003	81.618	1.276	72.664	10.230	24.555
5	2.39586	87.010	1.620	77.945	10.685	25.599
6	2.39141	85.003	1.880	80.553	6.330	15.138
7	2.39141	94.532	2.212	87.212	9.532	22.795
8	2.38696	99.333	2.464	94.428	7.369	17.590
9	2.3825	126.777	2.736	108.677	20.836	49.642
10	2.3781	124.928	2.792	112.665	15.055	35.802
11	No heat transferred					
12	2.36918	137.016	2.804	124.684	15.136	35.860
13	2.3647	155.225	2.752	136.123	21.854	51.678
14	2.3647	148.023	2.492	140.499	10.016	23.684
15	2.3603	157.251	2.024	148.795	10.480	24.736
16	2.35583	166.632	1.908	157.027	11.513	27.123
17	2.35583	175.265	1.648	164.700	12.213	28.772
18	2.3514	183.248	1.300	172.538	12.010	28.240
19	2.3514	185.505	0.936	176.452	9.989	23.488
20	2.3467	188.322	0.408	181.442	7.288	17.103
21	2.3425	190.688	0.348	186.139	4.897	11.471
22	1.000	189.944	0.200	186.936	3.208	3.208
23	2.3425	192.129	0.140	190.269	2.000	4.685

$$\sum_{1}^{23} q = 509.906 \times 6 = 3059.44 \text{ watts}/5^{\circ}\text{cut}$$

$$q_{refl} = 3059.44 \times 72 = 220{,}800 \text{ watts}$$

From $q = WC_p T$: $$T = \frac{(.2208 \times 10^6 \times 3.413)\text{BTU/hr}}{.188 \times 10^6 \text{ lb/hr} \times .3 \text{ BTU/lb}^{\circ}\text{F}} = \frac{0.75359}{0.0564} = \underline{13.36^{\circ}\text{F}}$$

[redacted]

[redacted]

[redacted] [redacted]

Appendix III

Total Gamma and Neutron Heat in Reflector

Slab	$\sum_{R_1}^{R_o} G$ / °F	24(Kt) / watts/°F	$q=24(Kt)\sum_{R_1}^{R_o} G$ / watts
1	4.352	32.918	143.261
2,20	7.906	57.607	455.443
3,19	11.062	57.607	637.251
4,18	13.877	57.607	799.415
5,17	16.920	57.5006	972.910
6,16	21.152	57.394	1213.99
7,15	22.501	57.394	1291.42
8,14	23.157	57.287	1374.89
9,13	29.492	57.180	1686.33
10,12	25.182	57.074	1437.24
21	6.253	56.328	352.23
22	3.939	24.096	94.914
23	2.178	56.220	122.48
11	--	--	1500.

$$\sum_{1}^{23} q = 21{,}950 \text{ watts}/^{o}5\text{cut}$$

$$Q_{Be} = \sum_{1}^{23} q' \times 72 = \underline{1{,}5804 \times 10^{6} \text{ watts}}$$

[redacted] [redacted]

Appendix IV

Neutron and Gamma Heating Within Reflector

G-w/cc	R-in →	N 1	N 2 20	N 3 19	N 4 18	N 5 17	N 6 16	N 7 15	N 8 14	N 9 13	N 10 12	N 11	N 21	N 22	N 23
18							9.38	10.12	10.66	11.07	11.28	10.99			
17						8.81	9.57	10.30	10.80	11.14	11.38	11.11			
16					8.05	8.95	9.72	10.44	10.92	11.25	11.48	11.20			
15					8.19	9.08	9.85	10.58	11.06	11.38	11.62	11.34			
14					8.33	9.22	10.00	10.73	11.22	11.55	11.78	11.50			
13				7.46	8.45	9.36	10.15	10.85	11.35	11.68	11.93	11.65			
12				7.59	8.64	9.55	10.33	11.02	11.50	11.84	12.09	11.80			
11				7.68	8.73	9.67	10.46	11.18	11.67	12.01	12.28	12.00			
10				7.83	8.90	9.83	10.62	11.34	11.73	12.15	12.43	12.16			
9			6.93	8.02	9.08	10.00	10.79	11.53	12.04	12.35	12.63	12.37			
8			7.19	8.28	9.33	10.24	11.04	11.79	12.32	12.65	12.92	12.62			
7		6.66	7.52	8.57	9.59	10.48	11.26	12.05	12.60	12.95	13.22	12.90	6.40		
6		6.95	7.88	8.93	9.90	10.83	11.60	12.40	12.95	13.30	13.53	13.21	6.70		
5		7.33	8.27	9.37	10.32	11.22	12.05	12.88	13.44	13.75	13.96	13.61	7.10		
4		7.90	8.85	9.90	10.89	11.80	12.63	13.42	13.96	14.23	14.45	14.12	7.65	6.62	
3		8.65	9.62	10.70	11.67	12.52	13.33	14.10	14.65	14.96	15.17	14.81	8.40	7.25	
2		9.90	10.82	11.95	12.92	13.75	14.48	15.16	15.68	15.95	16.17	15.77	9.65	8.60	7.[illegible]
1						16.40	17.03	17.55	17.81	18.00	18.12	17.64			

APPENDIX IV

ORNL-LR-DWG. 27092

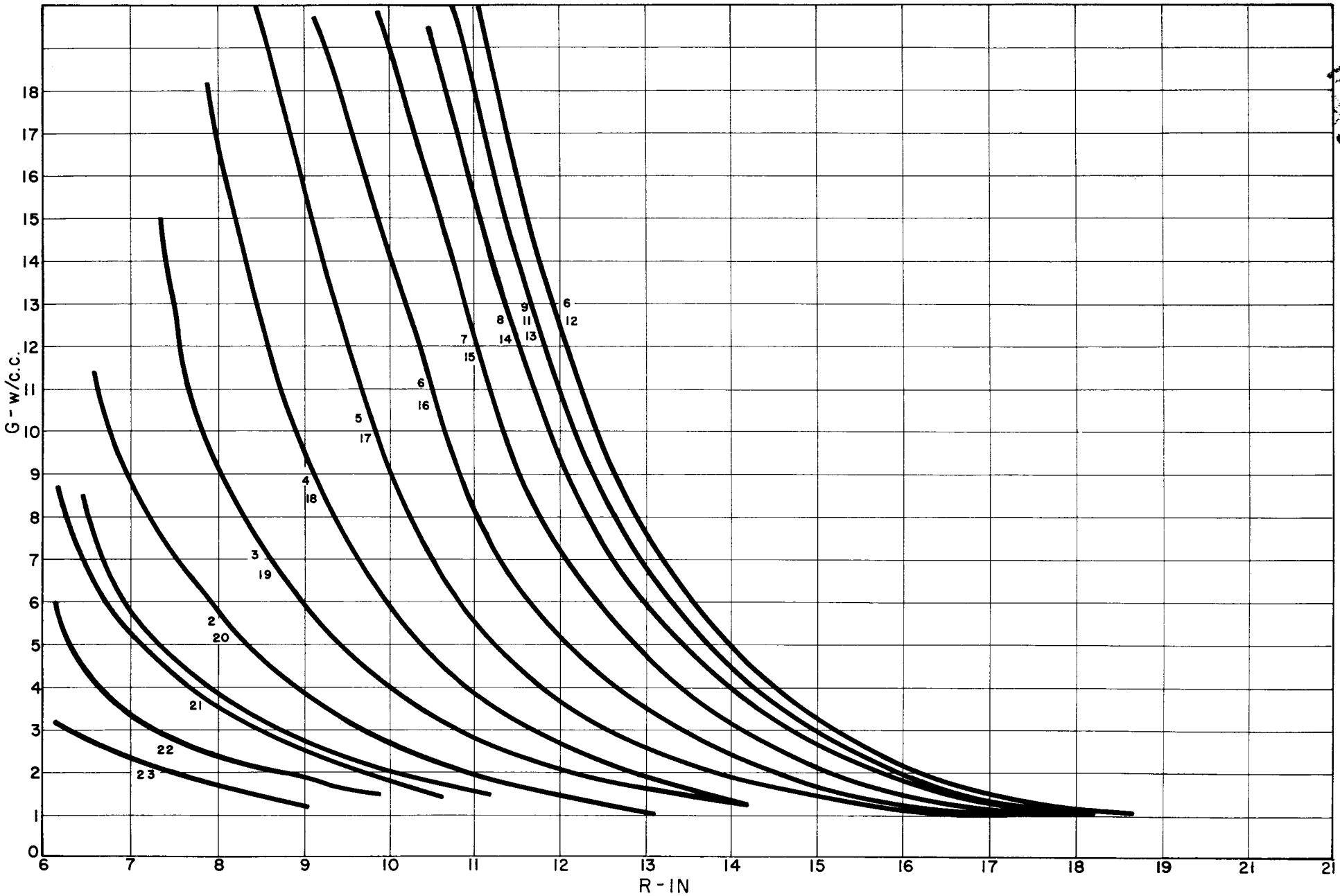

ORNL-LR-DWG. [redacted] 27091

THERMAL CONDUCTIVITY OF Be vs. TEMPERATURE

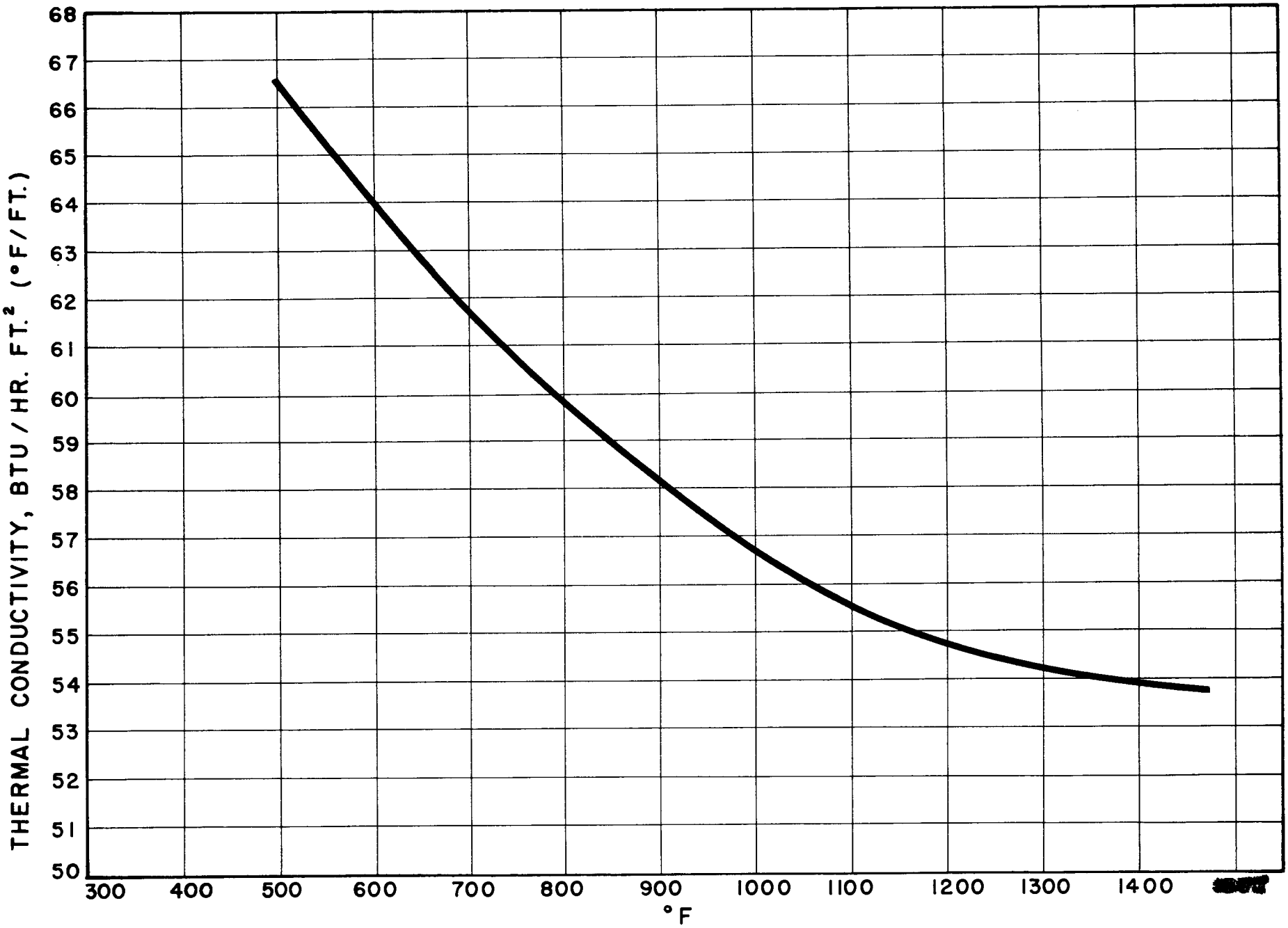

Appendix V

Slab Iteration

Row	W-lb/hr
Inside Annulus	0.188×10^6
1 (72 holes)	0.0186×10^6
2 (72 holes)	0.0205×10^6
3 (72 holes)	0.0251×10^6
4 (36 holes)	0.0134×10^6
5 (36 holes)	0.0134×10^6

Based on work by R. I. Gray.

Appendix V

$$q(\text{watts}) = (T_{op} + T_N + T_{N'} + G - 3T_o)xKt$$

Slab	Row 1	Row 2	Row 3	Row 4	Row 5
1 → 2	41.30	30.82	31.33		
2 → 3	104.87	83.12	99.95	65.79	
3 → 4	117.81	76.69	131.90	92.50	
4 → 5	253.69	177.12	173.35	133.92	
5 → 6	154.34	194.47	231.58	177.98	43.41
6 → 7	202.03	212.52	285.82	219.17	161.28
7 → 8	127.46	249.40	340.51	228.43	160.15
8 → 9	133.43	266.36	341.72	244.74	163.86
9 → 10	289.66	279.09	348.92	229.48	160.37
10 → 11	203.80	238.31	331.86	218.00	143.52
11 → 12	63.85	103.17	253.10	299.86	344.37
12 → 13	208.65	256.13	328.30	197.56	111.63
13 → 14	286.53	281.52	348.51	200.98	114.55
14 → 15	121.69	258.37	340.76	201.36	102.22
15 → 16	152.64	225.95	332.12	174.74	100.57
16 → 17	180.48	195.06	260.44	178.25	77.97
17 → 18	197.82	165.38	231.79	129.93	52.64
18 → 19	165.09	134.71	187.31	100.96	17.87
19 → 20	130.88	113.48	150.65	74.74	7.37
20 → 21	101.17	84.48	107.01	26.18	
21 → 22	66.46	66.41	73.06	15.69	
22 → 23	15.73	38.57	16.51		
23 → out	20.85	34.01	1.15		

Appendix V

$$T_{in}(n+1) = T_{out}(n) + \frac{q}{Wc_p}$$

Slab	Row 1	Row 2	Row 3	Row 4	Row 5
2	51.82	51.23	51.02	50.00*	
3	56.45	54.55	54.28	52.01	
4	61.64	57.62	58.59	57.67	
5	72.82	65.01	65.75	64.27	
6	79.62	72.78	73.31	75.13	142.65
7	88.52	81.27	82.64	88.55	152.51
8	94.13	91.24	93.76	102.52	162.30
9	100.01	101.89	104.91	117.48	172.32
10	112.77	113.04	116.30	131.51	182.13
11	121.75	122.56	127.13	144.84	190.91
12	124.56	126.68	135.39	163.18	211.97
13	133.65	136.92	146.11	175.26	218.80
14	146.27	148.17	157.49	187.55	225.80
15	151.63	158.50	168.61	199.86	232.05
16	158.35	167.53	179.45	210.54	238.20
17	166.30	175.33	187.95	221.44	242.97
18	175.01	181.94	195.52	229.38	246.19
19	182.28	187.32	201.63	235.55	245.10
20	188.05	191.86	206.55	240.12	244.65
21	192.51	195.24	210.04	241.72	
22	195.44	197.89	212.42	240.76	
23	196.13	199.43	212.96		
out	197.05	200.79	212.42		

$c_p = 0.3$ BTU/lb^{o}F

Appendix VI

External Sources of Heat to Inlet Na

I. Heat generated within Inconel support ring and B_4S plates

heating rates:

8 w/cm^{-2} - surface attenuation for B_4S and B_4Cu

3 w/cc - internal heating for B_4S and B_4Cu

1.5 w/cc - internal heating for Inc support ring.

(a) $Volume_{Inc} = 4833$ cc

$q_{Inc} = 1.5$ w/cc x 4833 cc = 7250 w

(b) Surface Area $B_4S = 2390\ cm^{-2}$

thickness $B_4S = 1$ cm

volume $B_4S = 2390\ cm^{-3}$

(1) $q(B_4S) = 8\ w/cm^{-2} \times 2390\ cm^{-2} = 19{,}120$ w

(2) $q(B_4S) = 3$ w/cc x 2390 cc = 7,170 w

$\Sigma q(B_4S + Inc) = 33{,}540$ w $= 11.4472 \times 10^4$ BTU/hr

$$\Delta T_{Na} = \frac{q}{c_p W} = \frac{11.4472 \times 10^4}{0.3 \times 1.34 \times 10^4} = \underline{28.5^\circ F}$$

Appendix VI

II. Heat generated within B_4Cu cone

thickness $_{B_4Cu}$ = 0.8128 cm

volume $_{B_4Cu}$ = 2038 cc

(a) $q_1 = \frac{8\ w/cm^{-2}}{0.8128\ cm} \times 2038\ cc = 20{,}059\ w$

(b) $q_2 = 3\ w/cc \times 2038\ cc = 6{,}114\ w$

$\Sigma q = 26{,}173\ w = 8.9328 \times 10^4$ BTU/hr

$$\Delta T_{Na} = \frac{8.9328 \times 10^4}{0.3 \times 1.34 \times 10^4} = \underline{22.2^oF}$$

III. Heat transferred from 1250°F Na return

$$q = \frac{0.14\ \frac{w}{cm^oF} \times 1105.6\ \overline{cm}^2 \times 185^oF}{0.635\ cm} = 4.5125 \times 10^4 w = 15.402 \times 10^4\ \text{BTU/hr}$$

$$\Delta T_{Na} = \frac{15.402 \times 10^4}{0.3 \times 1.34 \times 10^4} = \underline{38^oF}$$

$\Sigma \Delta T_{Na} \cong 90^oF$